Aalborg Universitet

Modelling and Design of Active Thermal Controls for Power Electronics of Motor Drive Applications

Ionuţ Vernica, and Frede Blaabjerg
Department of Energy Technology, Aalborg University
Pontoppidanstræde 101, 9220 Aalborg Øst, Denmark
Email: iov@et.aau.dk, and fbl@et.aau.dk

Ke Ma
School of Electronic Information and Electrical Engineering
Shanghai Jiao Tong University, Shanghai 200240, China
Email: kema@sjtu.edu.cn

Abstract—**One of the major factors that affects the overall efficiency and reliability of power electronics systems is the dynamical variation of the thermal stress which occurs in the power semiconductor devices. Therefore, the main objective of this paper consists of designing and implementing a series of active thermal control methods for the power devices of a motor drive application. The motor drive system together with the thermal cycling of the power devices have been modelled, and adverse temperature swings could be noticed during the start-up and deceleration periods of the motor. Based on the electrical response of the system, the junction temperature of the semiconductor devices is estimated, and consequently three active thermal control methods are proposed and practically designed with respect to the following parameters: switching frequency, deceleration slope and modulation technique. Finally, experimental results are provided in order to validate the effectiveness of the proposed control methods.**

Index Terms—**Thermal cycling, active thermal control, power device, motor drive system, temperature estimation.**

I. Introduction

Power electronics are being widely used in many mission-critical applications such as renewable power generation, power transmission, traction applications or motor drives, and due to their essential role within power systems, the reliability of the power converter is one of the main factors that influences the overall efficiency and cost of the system.

As a result, numerous studies have been carried out in order to identify the main causes of failure in power converters. In [1] it has been shown that the most fragile components of the power electronic system are the power semiconductor devices. According to [2]-[3], the high probability of failure in the power devices is primarily due to the thermal cycling which occurs in the device. These adverse temperature swings are mainly caused by the fluctuating load of the converter or environmental temperature variations, leading to some of the most common failure mechanisms which can appear in power modules, such as bond wire lift-off or solder cracks [4]-[5].

The aforementioned problems can also be frequently seen in motor drive applications, such as the study case discussed in this paper. During the start-up and braking periods of the motor, the large amplitude of the current and the fact that the machine operates at low fundamental frequency can lead to high temperature swings in the power semiconductor devices [6], which can quickly wear-out the connection inside the power devices, resulting in unsatisfied reliability performance and high cost of energy conversion.

Therefore, the analysis and control of the thermal loading of the power semiconductor devices is of great importance. An overview of the active thermal control techniques proposed throughout the literature is given in [7]. Various methods of controlling the junction temperature of power devices have been investigated, such as: switching frequency based hysteresis controller [8], region-based active thermal control [9] or modulation technique adjustment [10]-[11].

Unlike previously studied thermal control methods, where junction temperature feedback or complex controller design is required, within this paper an active thermal control technique based on the online junction temperature estimation of the power devices is proposed. In order to achieve the given objective, the motor drive model together with the thermal cycling of the power semiconductor devices is modelled, and the dynamic behaviour of the system is investigated under typical motor drive mission profiles. Based on the electrical response of the system, the junction temperature estimation of the transistor and the power diode is derived.

According to the estimated temperature of the devices, a thermal controller can thereby be designed in order to reduce the temperature swings which occur in the power semiconductor devices by adjusting the switching frequency, modulation technique or the deceleration slope. Finally, the simulation results are validated through experimental work.

II. Modelling of the Thermal Cycling in the Power Semiconductor Devices

A. Motor Drive Model

A typical motor drive application system is first designed as the study case. The system consists of a Permanent Magnet Synchronous Motor (PMSM) connect to the grid through a back-to-back three-level Neutral Point Clamped converter (3L-NPC), as shown in Fig. 1. The speed control of the motor is assured by means of Field Oriented Control (FOC), while the switching sequence of the power semiconductor devices of the converter is generated by a Sinusoidal Pulse Width Modulation (SPWM) technique. In this paper only the upper MOSFET (T_1) and the clamping diode (D_5) of the machine side converter will be analyzed. The parameters of the motor drive system
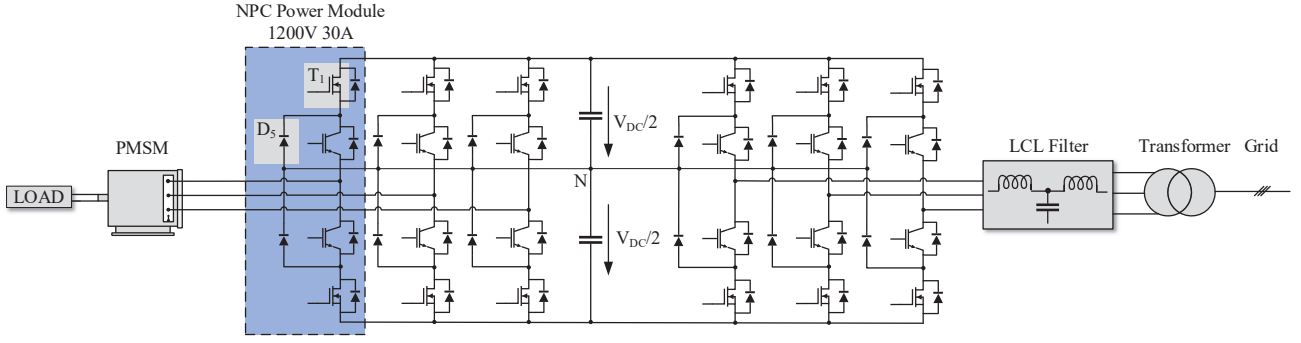
Fig. 1. Grid connected motor drive with back-to-back 3L-NPC.

are shown in Table I, while the power module choice is an IGBT module with a rated current of 30 A.

TABLE I. Motor drive parameters.

Parameter	Symbol	Value	Unit
Output Power	P_n	9200	[W]
Nominal Voltage	V_n	350	[V]
Max. Current	I_{max}	21.43	[A]
Nominal Torque	T_n	12.55	[Nm]
Inertia	J	0.011	[Kgm^2]
Nominal Speed	n_n	7000	[rpm]
Nr. Pole Pairs	n_{pp}	1	[-]
Supply Voltage	V_{ll}	400	[V]
Switching Frequency	f_{sw}	16	[kHz]

B. Power Loss Model

Based on the studies carried out in [12]-[14], it has been concluded that the total power losses of semiconductor devices are composed of conduction losses and switching losses. The conduction losses can be determined by using the following equation:

$$P_{\text{cond@}T_L/T_H} = V_{\text{cond@}T_L/T_H}(i_{abc}) \cdot i_{abc} \cdot d_{abc} \qquad (1)$$

where, $V_{\text{cond@}T_L/T_H}$ represents the conduction voltage of the power device at a certain low (T_L) or high (T_H) reference junction temperature, i_{abc} represents the three-phase current of the PMSM, and d_{abc} represents the duty cycle.

Similarly, the switching losses can be calculated as follows:

$$P_{\text{sw@}T_L/T_H} = f_{sw} \cdot E_{\text{sw@}T_L/T_H} \qquad (2)$$

where, f_{sw} represents the switching frequency and $E_{\text{sw@}T_L/T_H}$ is the switching energy of the device at a certain low (T_L) or high (T_H) reference junction temperature.

Due to the dependency between the loss characteristics and temperature, which was highlighted in [12]-[14], the junction temperature of the power device can be introduced as a feedback from the thermal model. Thus, the conduction or switching losses of the transistor or diode can be computed by using the following equation:

$$P_{\text{sw/con@}T_j} = \frac{P_{\text{sw/con@}T_H} - P_{\text{sw/con@}T_L}}{T_H - T_L}(T_j - T_L) + P_{\text{sw/con@}T_L} \qquad (3)$$

The total losses of the power semiconductor device can be found by adding together the conduction and switching losses.

$$P_{\text{device@}T_j} = P_{\text{cond@}T_j} + P_{\text{sw@}T_j} \qquad (4)$$

Finally, based on the power loss equations, the loss model can be build according to the block diagram shown in Fig. 2.

C. Thermal Model

As it has been shown in [15], both Foster and Cauer thermal network models have limited performance in terms of mapping the case temperature of the power semiconductor devices. Thus, a new hybrid thermal model proposed in [15] will be used in this paper. The RC thermal model is shown in Fig. 3, and it can be seen that it employs a multilevel RC Foster network in order to translate the power losses into the junction temperature of either the MOSFET or the power diode. The second path has slower dynamics, and by filtering the power losses through a low-pass filter, respectively by including the thermal network outside of the power module, the case and heat sink temperatures of the power devices can be determined.

The thermal resistance (R_i) and capacitance (C_i) used in modelling the Foster network have no physical meaning, and can normally be found in the device datasheet or can be determined by experimentally fitting the thermal impedance curve of the device.

$$Z_{\text{th(j-c)}} = \sum_{i=1}^{n} R_i(1 - e^{-\frac{1}{\tau_i}}) \qquad (5)$$

where, n represents the number of levels of the network and $\tau_i = R_i \cdot C_i$ represents the thermal time constant.
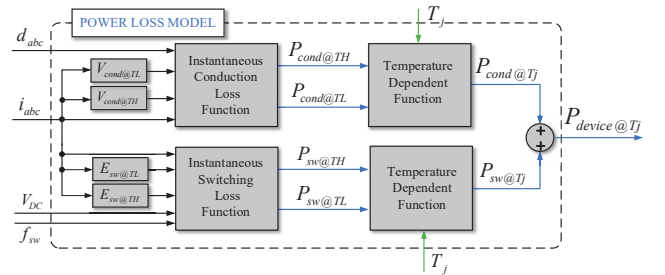

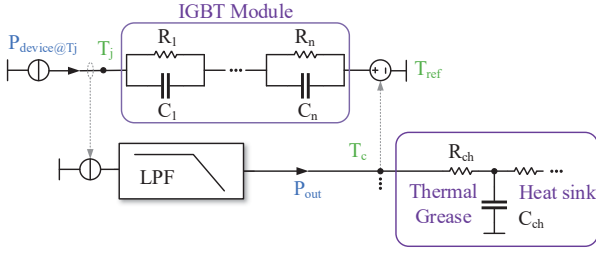Fig. 2. Average switching cycle power loss model diagram.

Fig. 3. RC Foster network used for thermal modelling.

D. Simulation Results

All the above mentioned models have been implemented in MATLAB/Simulink. The inputs to the system are the speed and torque mission profiles, which can be seen in Fig. 5, alongside the speed and torque response of the PMSM motor drive model. It can be noticed that the speed of the PMSM follows accurately the speed profile, indicating that the electrical model of the system together with its control have been modelled correctly. Similarly, from the current response of the machine plotted in Fig. 6, it can be noticed that, as expected, a high amplitude current is present at the terminals of the motor during the start-up and deceleration periods.

Due to the 3L-NPC inverter topology used in the present study case and due to its unequal current distribution among the power semiconductor devices, the current flowing through the upper MOSFET (T_1) and the clamping diode (D_5) placed on phase A of the machine side converter have been modelled.

The instantaneous and average current in the selected power devices is shown in Fig. 6. It can be observed that during the braking period of the PMSM, the amplitude of the average current through the transistor is almost null, most of the current flowing through its anti-parallel diode.
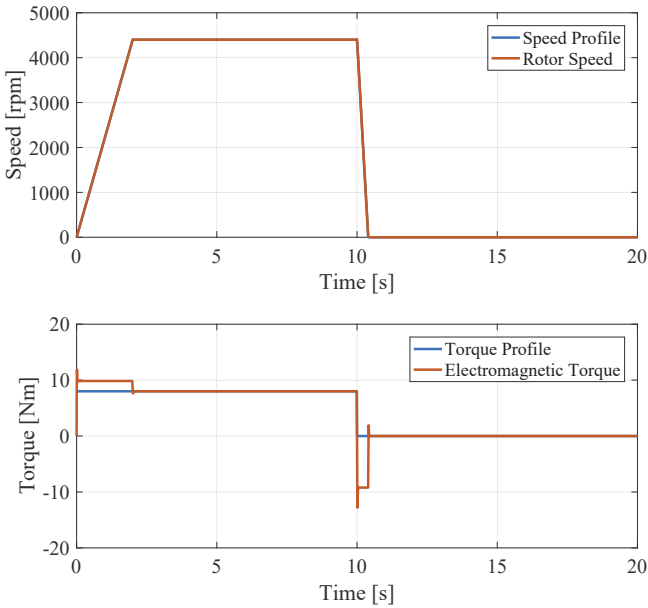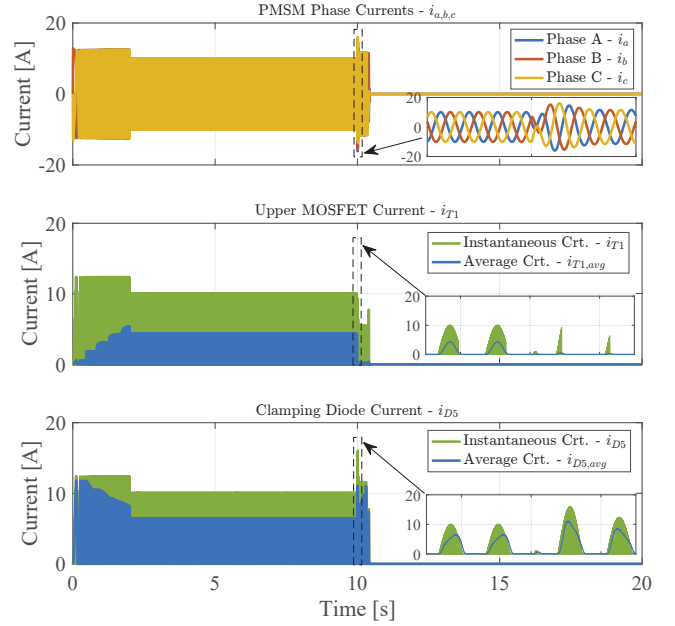

Fig. 6. Current flowing through the PMSM, T_1, and D_5.

On the other hand, more stress will be applied on the clamping diode due to the high amplitude current passing through the diode throughout the whole mission profile.

The average current flowing through the power devices will represent the input to the power loss model. Therefore, the total losses of the devices under the given design parameters and mission profiles are shown in Fig. 7. The strong dependency between the power loss distribution in the power devices and the power flow direction within the system can be highlighted: during the 'constant speed' period the power flows from the DC-link towards the PMSM, resulting in more stress on the

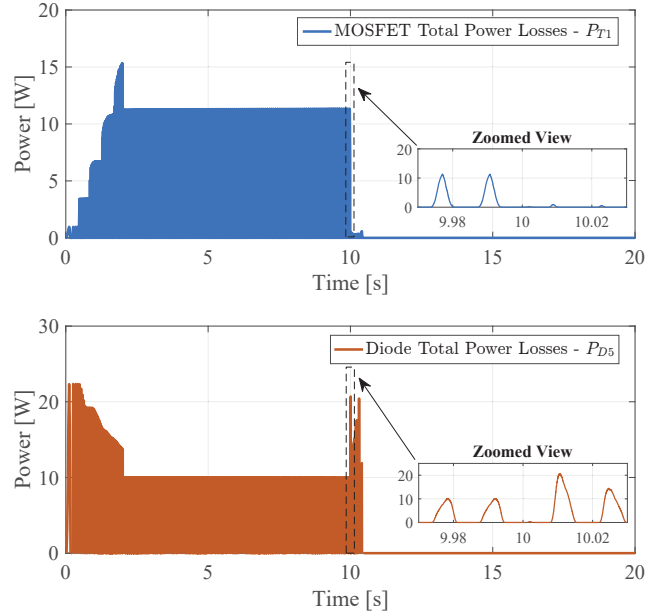Fig. 5. PMSM speed and torque input mission profiles.

Fig. 7. Device power losses under the given mission profiles.

transistor, while during the braking period, the PMSM will act as a generator, and the power will flow towards the DC-link, thus the clamping diode will be more stressed.

Finally, according to the input power losses of the devices and the estimated thermal parameters of the Foster network, the thermal cycles which appear in the power devices can be determined. At this point, it should be noted that an ambient temperature of $20^{o}C$ is taken into account during the thermal simulations. As it can be seen in junction temperature plot of the diode, presented in Fig. 8, some large temperature swings will occur during the start-up and deceleration periods of the motor, due to the large current amplitude and the low fundamental frequency operation of the converter. Similarly, during the 'constant speed' operation of the PMSM, the junction temperature will slowly increase due to the influence of the heat sink thermal dynamics.
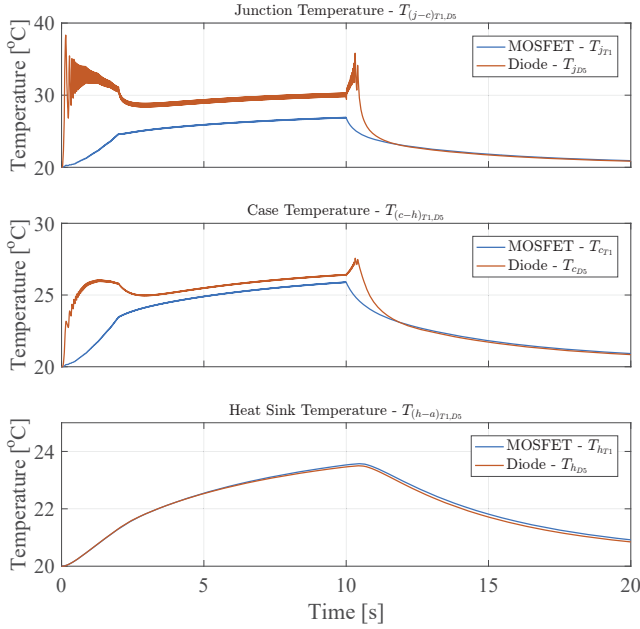

Fig. 8. Thermal loading of the power devices.

III. DESIGN OF ACTIVE THERMAL CONTROL METHODS FOR THE POWER DEVICES

In order to reduce the thermal cycle amplitude ΔT_j and mean value T_{jm} which occur in the power semiconductors throughout the whole mission profile (as highlighted in Fig. 4), three active thermal control methods are proposed within this paper. Due to the fact that the junction temperature of the devices is not always available for measurement and use within a thermal controller, an online junction temperature estimator is build. Based on the average power losses of the devices, the junction temperatures can be estimated according to the following equation:

$$T_{j,\text{est}_\text{T}} = \overline{P}_{\text{est}_\text{T}} \cdot R_{\text{th(j-c)}_\text{T}} + T_{\text{amb}} \qquad (6)$$

where, $R_{\text{th(j-c)}_\text{T}}$ represents the thermal resistance (junction to case) of the MOSFET given in the device datasheet, T_{amb} represents the ambient temperature, while the average power losses $\overline{P}_{\text{est}_\text{T}}$ can be estimated according on the equations presented in Section II. For a more accurate estimation, and in order to reduce the required computational power, the losses are filtered through a low-pass filter with a similar bandwidth as the thermal network, and the slow thermal dynamics of the heat sink (which takes into account the ambient temperature) is introduced. It should be noted that the same procedure can be applied for estimating the junction temperature of the freewheeling power diode of the machine side inverter.

The estimated thermal loading of the power devices is shown in Fig. 10, where it can be seen that the estimated junction temperature of the MOSFET follows accurately the thermal loading resulted from the developed thermal model. On the other hand, in case of the power diode, the thermal dynamics are correctly estimated, but some inaccuracies in terms of temperature cycle amplitude and mean value can be noticed during low frequency operation. Due to the nature of the thermal control which will be applied to the power diode junction temperature, these inaccuracies can be neglected.

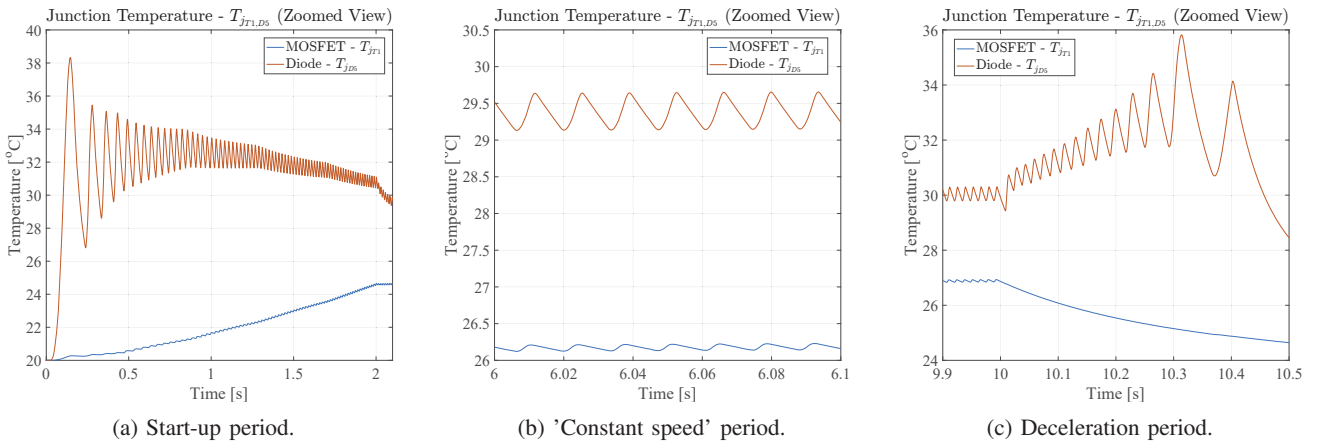(a) Start-up period. (b) 'Constant speed' period. (c) Deceleration period.

Fig. 4. Zoomed view of the junction thermal cycles of the power devices throughout the entire mission profile.
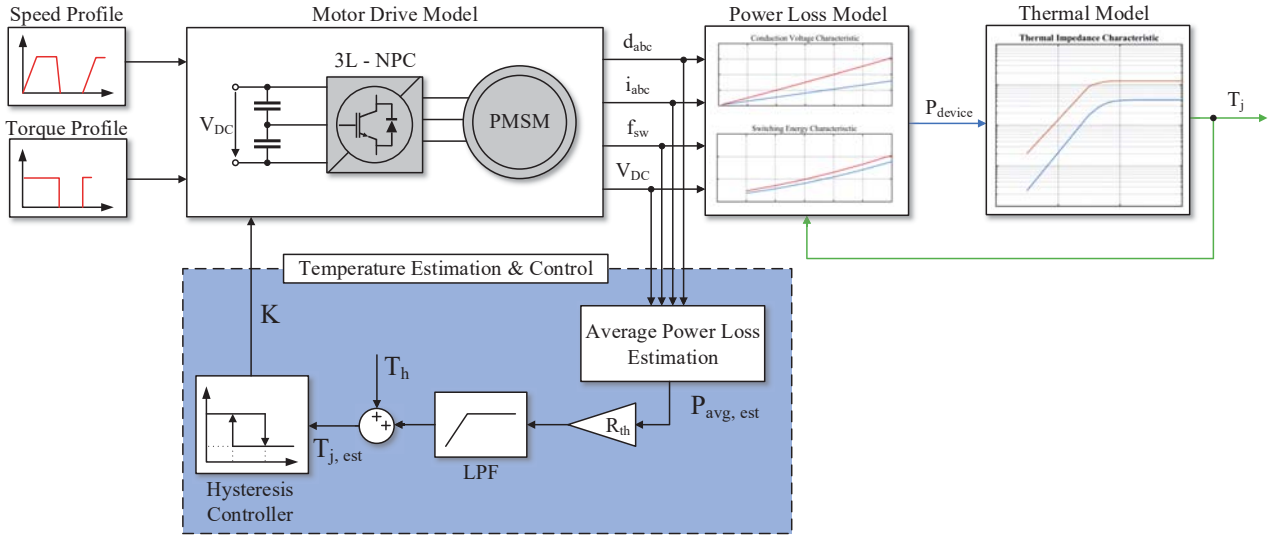
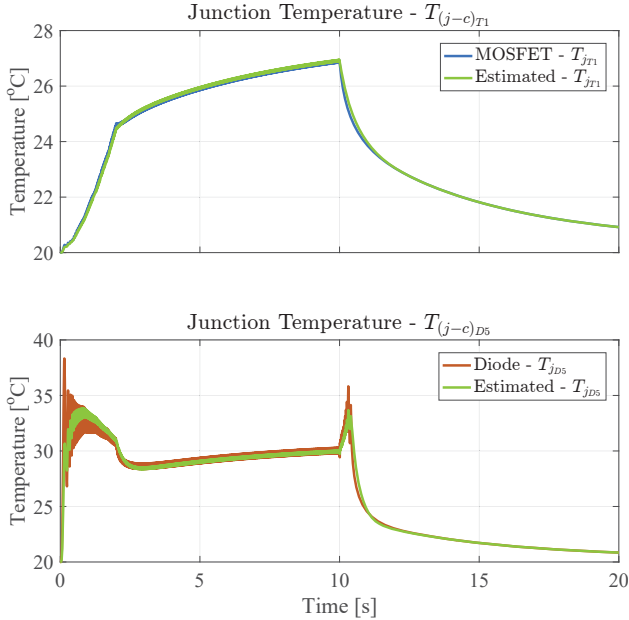Fig. 9. Generalized active thermal control method block diagram.

Fig. 10. Power device junction temperature estimation.

Once the thermal stress on the power devices has been correctly predicted, a hysteresis controller can be designed, and thus closing the thermal control loop, as shown in Fig. 9. The control parameter K represents the output of the hysteresis controller and it is determined by comparing the estimated junction temperature of the power semiconductor device to the temperature limits set by the controller. It should be noted that the control parameter K represents either the switching frequency, modulation technique or the deceleration slope, depending on the selected thermal control method.

$$K = \begin{cases} f_{sw}^* & \text{for } \textit{Switching Frequency Adjustment} \\ [1, 0] & \text{for } \textit{Modulation Technique Adjustment} \\ \omega^* & \text{for } \textit{Deceleration Slope Adjustment} \end{cases} \quad (7)$$

A. Switching Frequency Adjustment ($K = f_{sw}^*$)

By looking at the power loss equations it can be noticed that the switching frequency has a great influence on the switching losses generated by the power semiconductor devices, and inherently on their thermal loading. Therefore, by controlling the switching frequency of the inverter, the thermal cycling of the transistor can be significantly improved. On the other hand, the impact of this method on the thermal loading of the power diode is minor due to the small reverse recovery energy of the diode. Another drawback of this particular method is that, for motor drive applications, reducing the switching frequency can lead to higher current ripple, hence increasing the power losses on the PMSM [10].

The *Temperature Estimation and Control* block shown in Fig. 9, has been implemented in MATLAB/Simulink, and the hysteresis controller has been designed for adjusting the transistor thermal loading, with an upper temperature limit of $T_{lim,U} = 25^o C$ and a lower temperature limit of $T_{lim,L} = 23^o C$. Additionally, due to synchronisation reasons, the control parameter K can only have values multiple integers of the nominal switching frequency, thus $K \in \{16, 8, 4\} kHz$.

The effect of the *Switching Frequency Adjustment* thermal control method on the junction temperature of the power devices is shown in Fig. 11. It can be seen that after approximately 2.6 s, during the 'constant speed' operating period of the PMSM, the estimated junction temperature of the MOSFET reaches the upper limit of the hysteresis controller and the switching frequency is reduced to 8 kHz. Even though the thermal cycle amplitude of the transistor appears to be similar to the nominal operating case, a significant decrease in the mean value can be observed, resulting in an increased lifetime expectancy of the transistor. As expected, no major improvement on the thermal cycling of the freewheeling diode can be noticed for the given thermal control method.
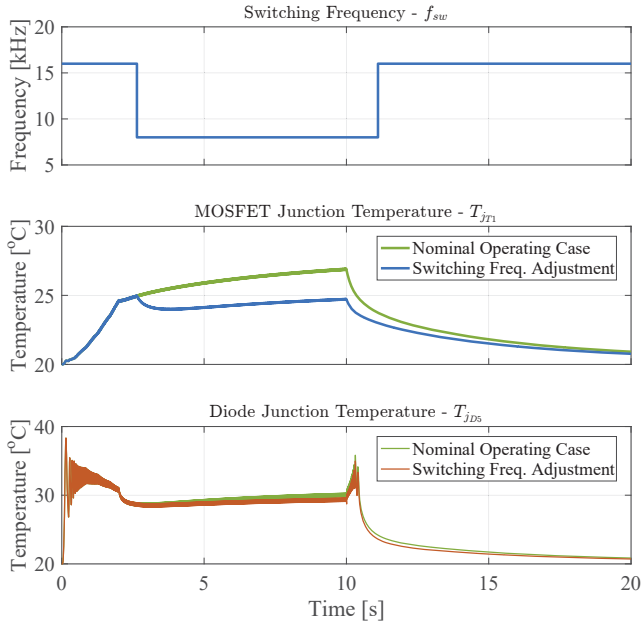
Fig. 11. *Switching Frequency Adjustment* - Thermal results.

B. Modulation Technique Adjustment

A similar thermal control method can be developed by adjusting the modulation technique used on the machine side inverter. The modulation technique chosen as an alternative to the SPWM method employed during the nominal operating case is the Discontinuous Pulse Width Modulation technique. The main reason for opting for DPWM1 is due to its reduced switching losses which occur on the active semiconductor devices, as a consequence to the fact that for 60° the modulation wave will be clamped [10], [16].
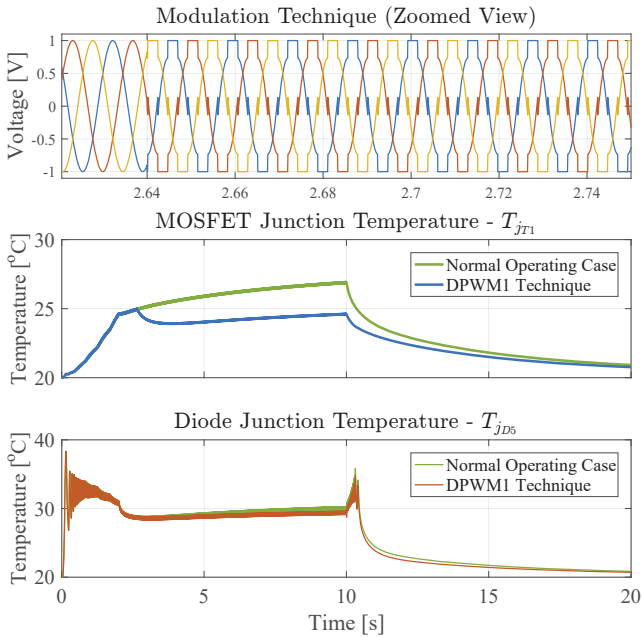

Fig. 12. *Modulation Technique Adjustment* - Thermal results.

The hysteresis controller has been modelled in a similar manner as for the *Switching Frequency Adjustment* method, with an upper temperature limit of $T_{lim,U} = 25^oC$ and a lower temperature limit of $T_{lim,L} = 23^oC$.

The junction temperature of the power devices resulting from the given thermal control method are plotted in Fig. 12, alongside the thermal loading of the devices under nominal operating conditions. Once the estimated temperature of the transistor reaches the upper limit of the controller, the modulation technique is switched from SPWM to DPWM1. It can be seen that the DPWM1 method has a slightly better performance in terms of reducing the thermal cycle mean value than the previously design method, but no major improvements can be noticed.

C. Deceleration Slope Adjustment ($K = \omega^*$)

One of the main parameters that affect the thermal loading of the power devices is the amplitude of the load current flowing through the power converter. Thus, the amplitude of the thermal cycles can be adjusted by controlling the output current of the PMSM. This can be achieved by increasing the deceleration slope of the speed mission profile, leading to a slow stop of the motor, and therefore a lower current amplitude during the braking period of the machine.

It should be noted that this method will have a higher impact on the freewheeling diode than on the upper transistor of the machine side converter. This is mainly due to the fact that during the braking period the electrical machine acts as a generator, and the power will flow from the PMSM towards the DC-link. Therefore, most of the current will pass through the freewheeling diode (D_5), and only a very small amount of current will flow through the transistor (T_1).

Consequently, the hysteresis controller has been designed in order to adjust the thermal cycling of the power diode, with with an upper temperature limit of $T_{lim,U} = 30^oC$.
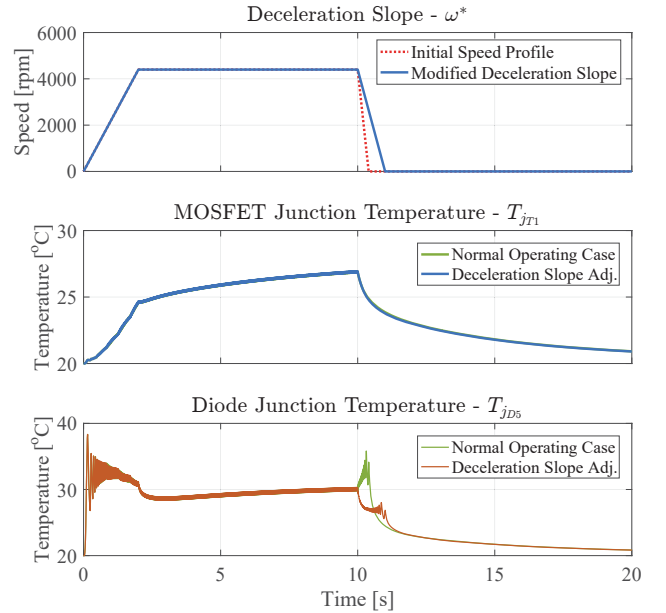

Fig. 13. *Deceleration Slope Adjustment* - Thermal results.

By decreasing the deceleration slope of the motor speed, the transition from operating state to full stop state of the PMSM will be more smooth, and will results a lower amplitude current generated during the braking period. Therefore, the power losses which occur on the power diode will be significantly reduced and will lead to lower thermal cycles amplitude and mean value, as shown in Fig. 13. As expected, this method has no influence on the thermal cycles of the MOSFET.

IV. EXPERIMENTAL VALIDATION

In order to validate the active thermal control methods, a dSpace-controlled 10 kW NPC H-bridge with an open IGBT module is being used. The setup allows the emulation of different mission profiles of various real-life applications, among which, motor drive systems. Therefore, the motor drive load conditions will be emulated on the inductive load of the setup and inherently on the power semiconductor devices of the 3L-NPC H-bridge. This will eliminate the need for an actual motor drive system, and will facilitate the measurement of the thermal behaviour of the power devices. The 'long-term' thermal cycles of the freewheeling diode and the upper transistor are obtained with an OpSens thermal fiber optic sensor system. The experimental setup is shown in Fig. 14.

Initially, the nominal operating conditions are emulated on the power module and the current and voltage response are shown in Fig. 15. It can be observed that the current flowing through the inductive load of the setup matches the simulated current loading of the PMSM. In Fig. 16, the thermal loading of the freewheeling diode and upper transistor of the 3L-NPC are shown. As expected, the thermal stress on the power diode is more severe than for the MOSFET. Similarly to the simulation results, some adverse thermal cycles can be noticed during the acceleration and deceleration periods, while during the 'constant speed' period the junction temperatures are slowly rising due the effects of the slow thermal dynamics of the case and heat sink.
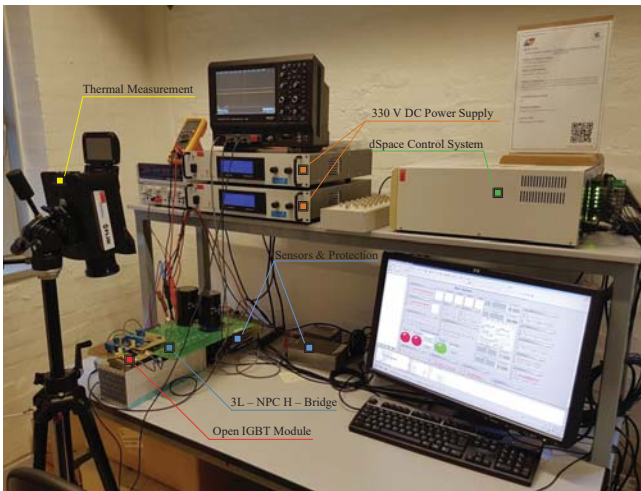

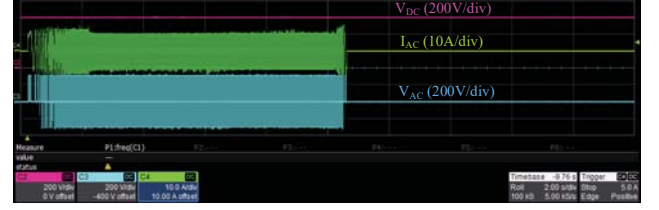Fig. 14. Mission profile emulator - Experimental setup.

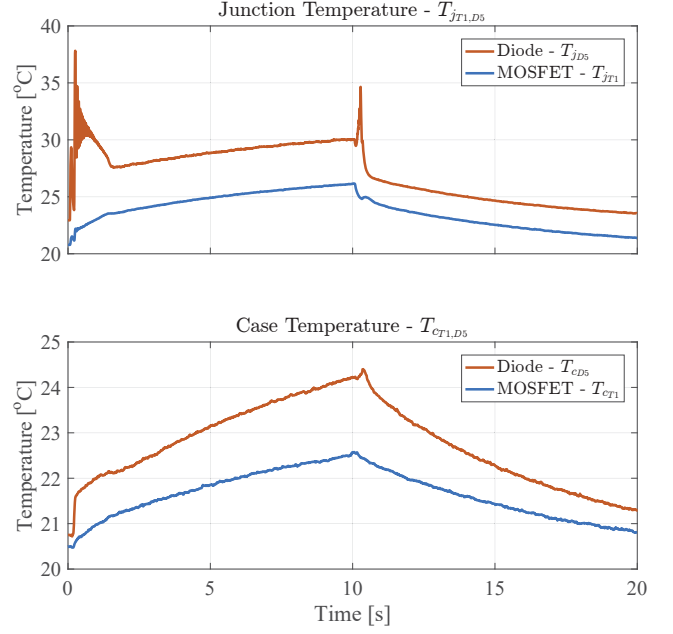Fig. 15. Electrical response for the nominal operating case.

Fig. 16. Device thermal dynamics - Nominal operating case.

Because of the low sampling frequency of the thermal measurement unit, the high frequency thermal cycles are not visible. Additionally, some minor inaccuracies might appear due the thermal coupling between the devices, factor which was not taken into consideration in the simulations. But, as it can be seen in Fig. 16, the experimental results fit well the simulation results in terms of cycle amplitude and mean value.

In the following, the *Deceleration Slope Adjustment* method has been implemented into dSpace. The resulting current and voltage mission profile can be seen in Fig. 17. The thermal response of the power semiconductor devices is shown in Fig. 18, where it can be seen that the thermal cycles which occur during the deceleration period in the freewheeling diode have been almost completely removed, in comparison with the nominal operating case.
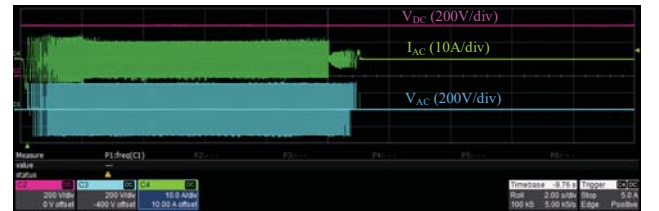

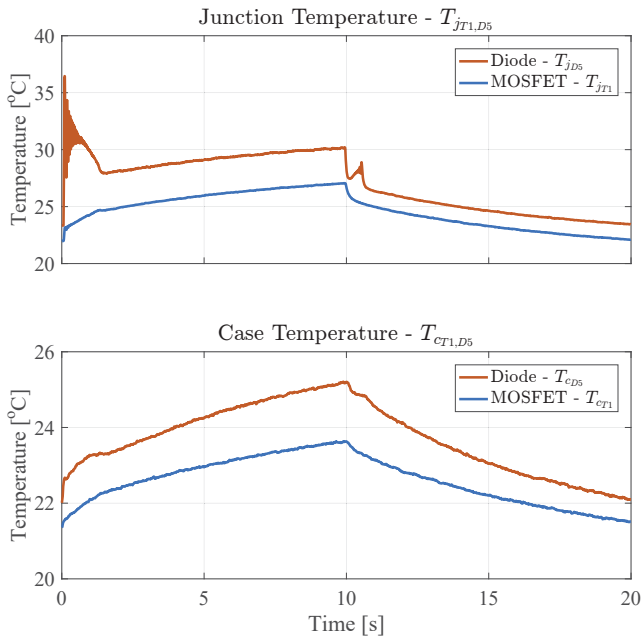Fig. 17. Deceleration Slope Adjustment - Mission profile.

Fig. 18. *Deceleration Slope Adj.* - Experimental Results.

V. Conclusions

In this paper the thermal behaviour of the power electronic devices of a motor drive system has been analyzed, and consequently three active thermal control methods have been proposed. The electrical model of the drive and thermal loading of the power devices have been modelled and investigated under given mission profiles. Based on the electrical parameter feedback, a simple and computational friendly power device junction temperature estimator has been designed. According to the estimated thermal loading of the devices a hysteresis controller has been implemented for each of the three thermal control methods: switching frequency adjustment, modulation technique adjustment and deceleration slope adjustment. The proposed thermal control methods have been investigated in terms of thermal cycle amplitude and mean value, and it has been concluded that the switching frequency and modulation technique can be successfully controlled in order to reduce the thermal loading of the transistor, while the deceleration slope adjustment methods has the most impact when controlling the freewheeling diode thermal stress. Finally, the thermal behaviour of the power devices under nominal operating conditions and deceleration slope adjustment have been validated through experimental work.

References

[1] S. Yang, A. Bryant, P. Mawby, D. Xiang, L. Ran, and P. Tav, "An Industry-Based Surveyof Reliability in Power Electronic Converters," *IEEE Trans. on Industry Applications*, vol. 47, no. 3, pp. 1441 - 1451, Jun. 2011.

[2] ZVEI: Die Elektroindustrie, *Handbook for Robustness Validation of Automotive Electrical/Electronic Modules*, German Electrical and Electronics Manufacturer Association, June 2013.

[3] M. H. Bierhoff, and F. W. Fuchs, "Semiconductor losses in voltage source and current source IGBT converters based on analytical derivation," in *Proc. of Power Electronics Specialists Conference*, vol. 4, pp. 2836 - 2842, 2004.

[4] U. M. Choi, *Thesis: Studies on IGBT Module to Improve the Reliability of Power Electronic Systems.* Aalborg: Aalborg University Press, Feb. 2016.

[5] V. Smet, F. Forest, J.-J. Huselstein, F. Richardeau, Z. Khatir, S. Lefebvre, and M. Berkani, "Ageing and Failure Modes of IGBT Modules in High-Temperature Power Cycling," *IEEE Trans. on Industrial Electronics*, vol. 58, no. 10, pp. 4931 - 4941, Oct. 2011.

[6] A. Wintrich, U. Nicolai, W. Tursky, and T. Reimann, *Semikron: Application Manual Power Semiconductors*, SEMIKRON International GmbH, 2015.

[7] M. Anderson, M. Liserre, and G. Buticchi, "Review of active thermal and lifetime control techniques for power electronic modules," in *Proc. of EPE*, Sept. 2014, pp. 1 - 10.

[8] J. Falck, M. Andresen, and M. Liserre, "Active thermal control of IGBT power electronics converters," in *Proc. of IECON*, Nov. 2015, pp. 1 - 6.

[9] D. A. Murdock, J. E. R. Torres, J. J. Connors, and R. D. Lorenz, "Active Thermal Control of Power Electronics Modules," *IEEE Trans. on Industry Applications*, vol. 42, no. 2, pp. 552 - 558, Mar. 2006.

[10] G. Lo Calzo, A. Lidozzi, L. Solero, F. Crescimbini, and V. Cardi, "Thermal regulation as control reference in electric drives," in *Proc. of EPE/PEMC*, Sept. 2012.

[11] M. Weckert, and J. Roth-Stielow, "Changes and limits of a thermal control for a 3-phase voltage source inverter in traction applications using permanent magnet synchronous or induction machines," in *Proc. of EPE*, 2011.

[12] M. Musallam, C. Yin, C. Bailey, and M. Johnson, "Mission profile based reliability design and real-time life consumption estimation in power electronics," *IEEE Trans. on Power Elect.*, vol.30, no.5, pp. 2601-2613, 2015.

[13] A. T. Bryant, P. A. Mawby, P. R. Palmer, E. Santi, and J. L. Hudgins, "Exploration of power device reliability using compact device models and fast electrothermal simulation", *IEEE Trans. on Industrial Applications*, vol.44, no.3, pp. 894 - 903, Jun. 2008.

[14] K. Ma, D. Zhou, and F. Blaabjerg, "Evaluation and design tools for the reliability of wind power converter system", *Journal of Power Elecronics*, vol.15, no.5, pp. 1149-1157, 2015.

[15] K. Ma, Y. Yang, and Frede Blaabjerg, "Transient modelling of loss and thermal dynamics in power semiconductor devices", *Proc. of IEEE ECCE*, pp. 5495 - 5501, 2014.

[16] M. Weckert, and J. Roth-Stielow, "Lifetime as a Control Variable in Power Electronic Systems," *Emobility - Electrical Power Train*, pp. 1 - 6, Nov. 2010.